Synthesis and Analysis of Primary High-Order Compensation Topologies for Wireless Charging System Applying Sub-Harmonic Control

Xiaoqiang Wang, Minrui Leng, Xin Zhang, *Senior Member, IEEE*, Hao Ma, *Senior Member, IEEE*, Bin Guo, Jianping Xu, *Member, IEEE*, and Chi-Kwan Lee, *Senior Member, IEEE*

***Abstract*— Subharmonic control (SHC) is an excellent method for wireless charging system because it is easy to achieve full-load range soft switching and unity power factor. However, in existing works, SHC is only applied to the system with primary series compensation topology, which has the drawbacks of low degrees of design freedom, high sensitivity to misalignments and no open-circuit protection. To overcome these issues, in this article, systematic synthesis of primary high-order compensation topology (PHCT) for WPT is identified in terms of general T-branch structure. Afterward, the applicability of PHCT to SHC is explored by gaining insight into their filter characteristics. It reveals that when SHC is applied, four kinds of PHCTs are superior over other candidates in performance because the unity power factor and soft switching can be achieved without limitation on pulse distribution. Then, six kinds of PHCTs exhibit a moderate performance as they may nullify the strengths of SHC under some specific pulse distributions. The rest of PHCTs are not applicable to SHC no matter what the pulse distribution. Finally, the experimental results on prototype with jointly applying SHC and PHCT are examined.**

***Index Terms*—Band-pass characteristics, primary high-order compensation topology (PHCT), subharmonic control (SHC), wireless charging system.**

Manuscript received 5 November 2022; revised 18 January 2023; accepted 18 February 2023. Date of publication 28 February 2023; date of current version 19 May 2023. This work was supported in part by the National Natural Science Foundation of China under Grant 52177198, in part by the Cao Guangbiao High-Tech Development under Grant 2020QN012, in part by the Delta Research and Education under Grant DREG2021002, and in part by the Hong Kong Research Grant Council under Theme-based Research Scheme under Grant T23-701/20-R. Recommended for publication by Associate Editor M. Ponce-Silva. *(Corresponding authors: Xin Zhang; Minrui Leng.)*

Xiaoqiang Wang, Xin Zhang, and Bin Guo are with the College of Electrical Engineering, Zhejiang University, Zhejiang 310027, China, and also with the Hangzhou Global Scientific and Technological Innovation Center, Zhejiang University, Hangzhou 310058, China (e-mail: xqwang06@zju.edu.cn; zhangxin_ieee@163.com; binguo_cr7@zju.edu.cn).

Minrui Leng is with the College of Electrical Engineering, Sichuan University, Chengdu 610065, China (e-mail: mrleng_pece@163.com).

Hao Ma is with the College of Electrical Engineering, Zhejiang University, Zhejiang 310027, China (e-mail: mahao@zju.edu.cn).

Jianping Xu is with the School of Electrical Engineering, Southwest Jiaotong University, Chengdu 610032, China, and also with the Key Laboratory of Magnetic Suspension Technology and Maglev Vehicle, Ministry of Education, Chengdu 610065, China (e-mail: jpxu-swjtu@163.com).

Chi-Kwan Lee is with the Department of Electrical and Electronic Engineering, The University of Hong Kong, 999077, Hong Kong (e-mail: cklee@eee.hku.hk).

Color versions of one or more figures in this article are available at https://doi.org/10.1109/TPEL.2023.3250396.

Digital Object Identifier 10.1109/TPEL.2023.3250396

I. Introduction

INDUCTIVE power transfer (WPT) technology [1], [2], [3], [4], [5] is able to deliver energy freely from power source to load through magnetic coupling without physical contact, realizing electrical isolation. Because of its inherent merits of safety, convenience and flexibility, WPT technology has gained in popularity for biomedical implants [2], electrified power trains [3], consumer electronics [5] and so on. Applying WPT to electric vehicles (EVs) is one of the most promising scenarios, it provides an easy way for charging EVs and extends the driving range. To enhance the efficiency of primary inverter and reduce electromagnetic interference in WPT systems, it is essential to realize zero voltage switching (ZVS) operation [4]. Also, the inherent protection characteristic is desired in case of the accidental open-circuit or the absence of EVs during the charging process [6].

In terms of power regulation, numerous control methods are reported to achieve battery charging for EVs [7], [8], [9], [10], [11]. Pulse width modulation including phase-shift (PS) control [7] and asymmetrical voltage cancellation [8] are adopted to regulate output power or voltage, but hard-switching on power devices cannot be avoided [4]. Although this problem can be solved by variable frequency (VF) control, high reactive power losses occur at light load [9]. As a compromise, VF plus PS hybrid control is used to achieve full-load range ZVS and improved power factor, but it comes at a cost of complicated current phase measurement [10], [11]. To address the above problems, a kind of "intermittent operation" method in a broad sense has been put forward. The so-called "intermittent operation" is based on controlling the ratio of a power-transfer interval of time with respect to a nonpower-transfer interval of time, such as burst mode [12], pulse density modulation (PDM) [13], [14], [15] and ON-OFF keying [16], [17]. The soft switching of PDM WPT system discussed in [13] depends on coupling coefficients and load conditions. In [14], an improved PDM is put forward by optimizing the distribution of switch sequences to reduce the current fluctuation of primary inverter. However, regarding to this "intermittent operation" method, the energy injected into resonant network is discrete and severe output voltage ripples is inevitable.

Fortunately, subhormonic control (SHC) [4], [18], [19], [20] is newly proposed to obtain full-load range ZVS and low output

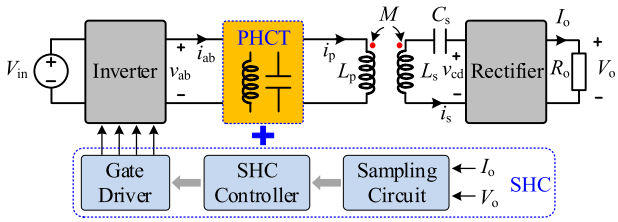

Fig. 1. Circuit diagram of WPT system applying PHCT and SHC.

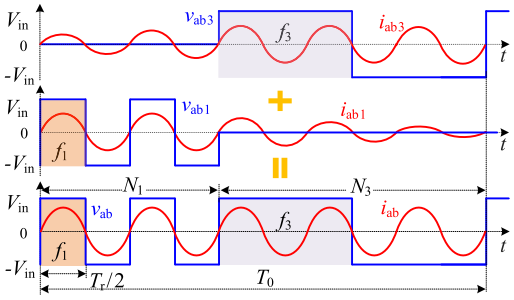

Fig. 2. Typical waveforms of SHC.

voltage ripples. It has been proven in [18] that the efficiency of WPT system with SHC can be improved by up to 5.68% as compared with its counterpart applying PS control. In [19], an optimal pulse arrangement algorithm for SHC is proposed to suppress the output voltage ripples. Experimental results show that the peak-to-peak voltage ripples is reduced to 2% and the efficiency improvement of SHC occurs under light load which is up to 17.8% than PS control. However, in existing works, the implementation of such control is mainly based on the primary series compensation topology (PSCT). That is because PSCT exhibits an excellent band-pass characteristic, which is also the prerequisite of SHC. However, as indicated in [15], PSCT has some shortcomings: the first one is low design freedom of coupling coils and the second is high sensitivity to coil misalignments. This means that the system may be destroyed by large current and power flowing through primary coil when the accidental open-circuit or the absence of EVs occur during the charging process. To overcome the shortcomings, primary high-order compensation topology (PHCT) is explored in the literature. An inductor-capacitor-capacitor (LCC) topology and a series-parallel (SP) topology are reported in [21] and [22], respectively. A family of high-order compensation topologies are analyzed to achieve load-independent voltage and current characteristics [23], [24]. Apparently, PHCTs provides more design freedom and can make the output voltage and/or current controllability.

If the WPT system can take advantage of the respective strength of PHCT and SHC, the overall performance would be improved significantly. However, there are strict requirements on PHCT when applying SHC because SHC exhibits a wide spectrum distribution and a narrow band-pass characteristic for WPT system is necessary. Thus, exploring the possibility of PHCT applying SHC is imperative, which has not been carried out yet.

To fill the technical gap mentioned above, in this article, the synthesis and analysis of PHCT are investigated in terms of a general T-branch structure. In all, 29 PHCTs are classified into four types, which are able to provide load-independent output and inherent open-circuit protection. Afterward, the possibility of PHCT applying SHC is further identified by gaining insight into the filter characteristic of WPT system. Among the newly derived PHCTs, it reveals that when SHC is used, four kinds of PHCTs are superior over other candidates in performance because the unity power factor and soft switching can be achieved without limitation on pulse distribution. Second, six kinds of PHCTs exhibit a moderate performance since they may nullify the strengths of SHC with some specific pulse distributions. This phenomenon is caused by the steep band of PHCT. The rest of PHCTs, including the popular *LCC* [21], SP [22], and CLC topologies [27], etc., are not practicable to SHC no matter what the pulse distribution is. The major contribution of this article is first exploring the interrelation of PHCT and SHC when they are jointly applied in a WPT system. A systematic synthesis and classification of PHCTs are also provided to guide the engineers and researchers for topology selection and design.

II. Analysis of SHC

In this section, operation principle and typical waveforms of SHC is presented. Also, the spectrum analysis is provided to illustrate its harmonic distribution. To make the receiver more compact, single-capacitor compensation is employed. Fig. 1 shows the diagram of WPT system applying PHCT and SHC, which can take advantage of their respective strengths. Thus, the overall performance of WPT system is greatly improved.

A. Operation Principle

The basic principle of SHC is to adjust the numbers of different frequency pulses of inverter to change the equivalent voltage gain. Detailed explanation and analysis on SHC can be given in [18], [19], and [20]. For the ease of understanding, taking f_1 and f_3 pulses as an example, the typical waveforms are shown in Fig. 2, where $f_1 = 3f_3$, the pulse numbers of f_1 and f_3 are, respectively, N_1 and N_3. $T_r = 1/f_r = 1/f_1$ is resonant period, and $T_0 = (N_1T_r + 3N_3T_r)/2$ is the SHC period. The output voltage and current of inverter are denoted as v_{ab} and i_{ab}, respectively. V_{in} is the input dc voltage.

According to superposition theorem, the resonant current i_{ab} is generated by two excitation voltages, i.e., v_{ab1} and v_{ab3} with f_1 pulses and f_3 pulses, as shown in Fig. 1. As pointed in [4], the prerequisite of SHC is a narrow band-pass characteristic of the WPT system. Thus, only v_{ab1} and the third-order harmonic of v_{ab3} contribute to resonant current i_{ab}. The amplitude of the fundamental component of v_{ab}, denoted as $V_{ab,p}$, is calculated as

$$V_{ab,p} = \frac{N_1 + N_3}{N_1 + 3N_3} \frac{4V_{\text{in}}}{\pi}. \tag{1}$$

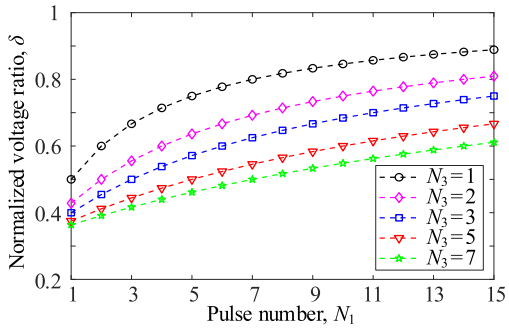

Fig. 3. Normalized voltage ratio δ against different N_1 and N_3.

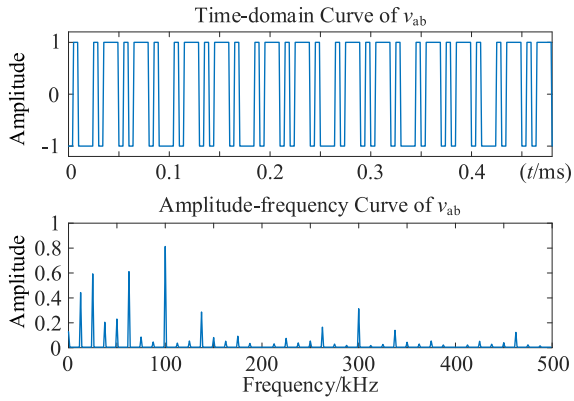

Fig. 4. DFT results of v_{ab} with $N_1 = 7$, $N_3 = 3$ by using MATLAB.

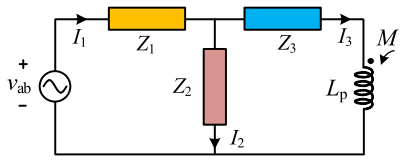

Fig. 5. Circuit diagram of PHCT with T-structure configuration.

Taking $4V_{\text{in}}/\pi$ as reference voltage, the normalized voltage ratio δ is given as

$$\delta = \frac{N_1 + N_3}{N_1 + 3N_3}. \tag{2}$$

According to (2), the normalized voltage ratio with different N_1 and N_3 is shown Fig. 3. It can be found that δ increases as N_1 increases when N_3 is constant. However, when N_1 is fixed, δ decreases as N_3 increases.

B. Spectrum Components

As indicated before, the prerequisite of SHC is a narrow band-pass characteristic of the WPT system, dominating the suitability of PHCTs. To better evaluate the performance of PHCTs in Section III, the spectrum components of inverter voltage v_{ab} should be identified firstly. The harmonic concept is based on Fourier analysis whose motivation is to reconstruct the nonsinusoidal periodical waveshape by a series of sinusoidal components [25]. As shown in Fig. 2, v_{ab}(t) is a continuous periodical signal with period of T_0 and it satisfies Dirichlet condition. Consequently, it can be represented by a Fourier series of

$$v_{ab}(t) = \sum_{n=-\infty}^{\infty} X(n\omega_0)\, \mathrm{e}^{\mathrm{i}n\omega_0 t} \tag{3}$$

where $\omega_0 = 2\pi/T_0$ is called fundamental frequency, and $X(n\omega_0)$ is the Fourier coefficient at the nth harmonic.

To satisfy system oscillation frequency invariance, $N_t = N_1 + 3N_3$ should be even. Due to the fact that a complete control period T_0 includes several resonant cycles, the spectrum of v_{ab} contains both subharmonics and interharmonics [18], [28]. As a consequence, the harmonics positions can be given by

$$f_j = \left(1 \pm \frac{j}{N_t}\right)(2n-1)\, f_r, j = 1, 2, \ldots, N_t - 1. \tag{4}$$

To push the harmonics far away from f_r and filter them with the band-pass characteristics of WPT system, sigma-delta (Σ-Δ) modulation is widely used, which can be referred in [4] and [19]. Since the amplitude of harmonics is related to the hybrid pulse sequence and pulse numbers N_1 and N_3, it is impossible to derive the analytical expression. For the convenience of Fourier analysis, discrete Fourier transform (DFT) could be applied [25]. As an example, Fig. 4 shows the DFT results of v_{ab} with $N_1 = 7$, $N_3 = 3$ by using MATLAB. It can be observed that the spectrum components are consistent with the theoretical prediction in (4). If the spectrum components of voltage v_{ab} are determined, it is helpful to evaluate the performance of PHCT combining SHC and this will be analyzed in the following section.

III. Synthesis and Derivation of PHCTs

Before exploring the combination of PHCT and SHC, the possible PHCTs should be identified. Most importantly, the candidates of PHCT should avoid the drawbacks of PSCT, i.e., low degree of design freedom, no open-circuit protection and high sensitivity to misalignments. Based on these objectives, the synthesis procedure of PHCT starts with the general T-branch structure. The search is restricted to a maximum of two reactive elements in each branch since more reactive elements increase the size, weight, and cost of system and complicate the analysis and design.

A. Topology Synthesis

Generally, voltage-fed inverter is widely employed in WPT systems and thereby PHCT can be configured by a T-branch structure, as shown in Fig. 5. Each branch has an impedance Z_i ($i = 1, 2, 3$), and the corresponding branch current is I_i. L_p is the primary coil inductance, and M is the mutual inductance. Z_{in} is the input impedance. To maximize the transfer efficiency, it is preferred to fully compensate the secondary coil at the resonant frequency f_r. Therefore, the loading effect of the secondary on the primary circuit can be presented by a reflected impedance

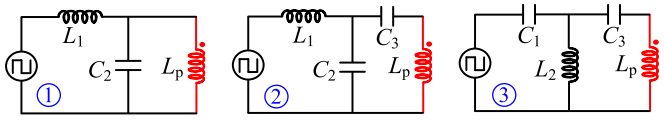

Fig. 6. Circuit diagram of type I PHCT candidates.

Z_f, which is pure resistive as

$$Z_f = \frac{\omega_r^2 M^2}{R_{\rm ac}} \tag{5}$$

where $R_{\rm ac}$ is the equivalent ac load [4] and $\omega_r = 2\pi f_r$.

Then, the WPT system shown in Fig. 5 can be described as

$$\begin{cases} Z_{{\rm in}(r)} = Z_{1(r)} + \frac{Z_{2(r)}\left(Z_{3(r)}+j\omega_r L_p+Z_f\right)}{Z_{2(r)}+Z_{3(r)}+j\omega_r L_p+Z_f} \\ I_{3(r)} = \frac{V_{ab(r)}}{Z_{{\rm in}(r)}} \frac{Z_{2(r)}}{Z_{2(r)}+Z_{3(r)}+j\omega_r L_p+Z_f} \end{cases} \tag{6}$$

where the subscript "$_{(r)}$" represents the corresponding variables at the resonant frequency f_r.

In addition to the band-pass characteristic of PHCT, there are some objectives that should be fulfilled to promote the overall performance of WPT system. The first one is the unity power factor operation, which aims to minimize the voltage-ampere rating of power supply and devices. The second one is the load-independent output voltage, which is able to reduce the regulation complexity. The third one is the inherent protection in case of the accidental open-circuit or the absence of receiver. This means the input impedance should be infinite when the coupling tends to zero. Combing these requirements and (6), it is easy to get

$$\begin{cases} \boldsymbol{Im}\left(Z_{{\rm in}(r)}\right) = 0 \\ Z_{1(r)} + Z_{2(r)} = 0 \\ Z_{{\rm in}(r)}\big|_{Z_f \to 0} = \infty \end{cases} \Rightarrow Z_{1(r)} = -Z_{2(r)} = Z_{3(r)} + j\omega_r L_p. \tag{7}$$

The symbol ***Im*** returns the imaginary part of the variables. From (7), it can be observed that all branch reactance should be equal. Note that the reactance of Z_3 branch includes the reactance of L_p. if Z_1 branch and Z_2 branch are inductive (or capacitive), Z_3 should be capacitive (or inductive). Placing reactive elements (inductors and capacitors) in place of Z_i in Fig. 5, consistent with the definition of PHCT and simultaneously satisfying the condition expressed in (7), a family of PHCTs can be synthesized. Please note that Z_i is constrained to be composed of a maximum of two reactive elements to restrict the maximum number of reactive elements in a network to six. Also, Z_i can be considered to be composed of more reactive elements to further explore higher order topologies, if desired.

To make a methodical synthesis, in this article, we defined four types of PHCTs in terms of the configuration of reactive elements.

1) *Type I:* Only single capacitor or inductor exists in Z_i, as shown in Fig. 6. Please note that if the Z_3 block in Fig. 4 is replaced by an *LC* series network, the compensation inductor can be merged into L_p forming a lower order network. In circuit theory, capacitors cannot in parallel with square-wave voltage source otherwise large current spikes will flow during the switching transitions. For example, if the inductor L_1 in Type I-1 is replaced by a capacitor, a voltage source capacitor loop will be formed and this case is strictly forbidden. Besides, the constraint expressed in (7) also remove some candidates. For instance, if the capacitor C_3 in types I–3 is omitted, it is allowed in term of circuit theory. However, this would make Z_1 branch be capacitive while Z_3 branch be inductive, which is against (7). In all, three type I PHCT candidates are obtained. Obviously, type I-1, type I-2, and type I-3 PHCTs are widely explored in the literature, which are also named as LC [26], *LCC* [10], [15] and *CLC* topologies [27], respectively.
2) *Type II:* At least one *LC* series network exists in Z_i, but without *LC* parallel network, as illustrated in Fig. 7. Taking all abovementioned constraints into consideration, eight type II PHCT candidates are finally developed.
3) *Type III:* At least one *LC* parallel network exists in Z_i, but without *LC* series network, as shown in Fig. 8. In this case, the inductor L_2 in type III-3 cannot be merged into L_p directly because L_p is coupled with the secondary coil and thereby a controlled voltage source exists in Z_3 branch. In a similar way, seven type-III PHCT candidates are identified.

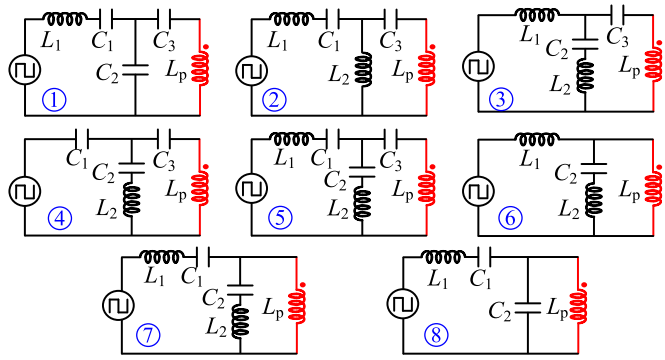

Fig. 7. Circuit diagram of type II PHCT candidates.

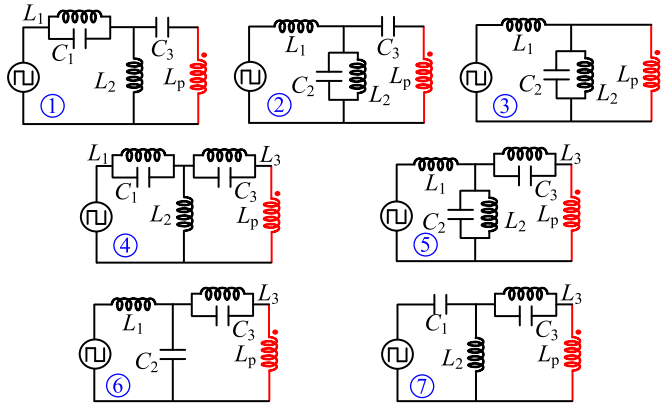

Fig. 8. Circuit diagram of type III PHCT candidates.

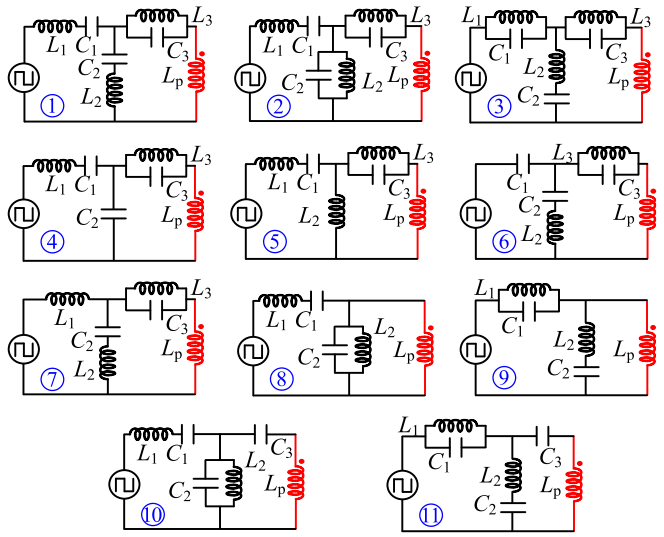

Fig. 9. Circuit diagram of type IV PHCT candidates.

4) *Type IV:* At least one hybrid network, i.e., one *LC* series network and one *LC* parallel network, exists in Z_i, as shown in Fig. 9. Due to the increased order of PHCT, there may be more degree of freedom in branch impedance configuration. As an example, the Z_1 and Z_3 branches in type IV-1 (and 2, 3, 10, 11) can be inductive (or capacitive) and Z_2 branch is capacitive (or inductive). Such two cases also exist in type II-5 topology. For the convenience of identification, when Z_1 branch in PHCT is inductive, we refer to it as type IV-1A, otherwise, it is called as Type IV-1B. This definition is also available to other similar PHCTs, such as type II-5A and type II-5B, etc.

The PHCTs in Figs. 6–9 possess the characteristics of unity power factor, inherent open-circuit protection and load- independent output only if the condition expressed in (7) is satisfied. When the system operates at resonant frequency, the reactance of Z_1 branch and Z_2 branch can be equivalent to an inductor L_E or a capacitor C_E, that is

$$|Z_{1r}| = |Z_{2r}| = \omega_r L_E = \frac{1}{\omega_r C_E}. \tag{8}$$

For simplicity, the following terms are defined: Normalized switching frequency $f_n = f/f_r$; Ratio of inductances $\alpha_i = L_i/L_E$ and $\gamma = L_p/L_E$; ratio of capacitances $\beta_i = C_i/C_E$. The compensation inductors L_i and capacitors C_i ($i = 1, 2, 3$) are shown in Figs. 6–9. Table I summarizes the design conditions in terms of the relationship among the values of reactive elements (i.e., α_i, β_i, and γ). For example, α_1 in type I-1 topology represents the ratio of L_1 and L_E, and β_2 in type I-1 topology represents the ratio of C_2 and C_E, and so on.

B. Combination of PHCT and SHC

To identify the practicability of PHCT when applying SHC, the band-pass characteristic of WPT system should be studied. In following analysis, several assumptions serve as premises for a fair comparison: resonant network is lossless, switch components are ideal and the parameters of secondary side and the mutual inductance for all PHCTs are same.

Input admittances of PHCTs are derived for the analysis of filter characteristics. Due to the limited space of this article, the band-pass characteristics of only four representative PHCTs are explored in detail. Table II gives the specifications of WPT system with different PHCTs.

According to the analysis in Section II-B, the harmonic of excitation voltage versus different δ (with Σ-Δ modulation) are shown in Fig. 10. As indicated in (2), δ can be derived from N_1 and N_3. In Fig. 10, the colors of markers represent different

TABLE I
DESIGN CONDITIONS OF PHCTS

Type I-1	Type I-2	Type I-3	
$\alpha_1\beta_2=1$, $\alpha_1=\gamma$	$\alpha_1\beta_2=1$, $\alpha_1+1/\beta_3=\gamma$	$\beta_1\alpha_2=1$, $\alpha_2+\gamma=1/\beta_3$	–
Type II-1	Type II-2	Type II-3	Type II-4
$\alpha_1+1/\beta_2=1/\beta_1$ $\gamma+1/\beta_2=1/\beta_3$	$\alpha_1+\alpha_2=1/\beta_1$ $\gamma+\alpha_2=1/\beta_3$	$\alpha_1+\alpha_2=1/\beta_2$ $\alpha_1+1/\beta_3=\gamma$	$1/\beta_1+1/\beta_2=\alpha_2$ $1/\beta_1+\gamma=1/\beta_3$
Type II-5	Type II-6	Type II-7	Type II-8
$\alpha_1+\alpha_2=1/\beta_1+1/\beta_2$ $1/\beta_1+\gamma=\alpha_1+1/\beta_3$	$\alpha_1+\alpha_2=1/\beta_2$ $\alpha_2+\gamma=1/\beta_2$	$\alpha_1+\alpha_2=1/\beta_1+1/\beta_2$ $\alpha_2+\gamma=1/\beta_2$	$\alpha_1+1/\beta_2=1/\beta_1$ $1/\beta_2+\gamma=0$
Type III-1	Type III-2	Type III-3	Type III-4
$\alpha_1/\alpha_2+1=\alpha_1\beta_1$ $\alpha_2+\gamma=1/\beta_3$	$\alpha_2/\alpha_1+1=\alpha_2\beta_2$ $\alpha_1+1/\beta_3=\gamma$	$\alpha_2/\alpha_1+1=\alpha_2\beta_2$ $\alpha_1=\gamma$	$\alpha_1/\alpha_2+1=\alpha_1\beta_1$ $1+\alpha_1/(\alpha_2+\gamma)$ $=\alpha_3\beta_3$
Type III-5	Type III-6	Type III-7	
$\alpha_2/\alpha_1+1=\alpha_2\beta_2$ $1+\alpha_3/(\gamma-\alpha_1)$ $=\alpha_3\beta_3$	$\alpha_1\beta_2=1$, $1+\alpha_3/(\gamma-\alpha_1)$ $=\alpha_3\beta_3$	$\alpha_1\beta_2=1$, $1+\alpha_1/(\alpha_2+\gamma)$ $=\alpha_3\beta_3$	–
Type IV-1	Type IV-2	Type IV-3	Type IV-4
$\alpha_1+\alpha_2=1/\beta_1+1/\beta_2$	$1+\alpha_2/(\alpha_1-1/\beta_1)=\alpha_2\beta_2$	$1+\alpha_1/(\alpha_2-1/\beta_2)$ $=\alpha_1\beta_1$	$\alpha_1+1/\beta_2=1/\beta_1$
$1+\alpha_3/(\gamma-\alpha_1+1/\beta_1)=\alpha_3\beta_3$	$1+\alpha_3/(\gamma-\alpha_1+1/\beta_1)=\alpha_3\beta_3$	$1+\alpha_3/(\gamma+\alpha_2-1/\beta_2)=\alpha_3\beta_3$	$1+\alpha_3/(\gamma-1/\beta_2)$ $=\alpha_3\beta_3$
Type IV-5	Type IV-6	Type IV-7	Type IV-8
$\alpha_1+\alpha_2=1/\beta_1$ $1+\alpha_3/(\gamma+\alpha_2)$ $=\alpha_3\beta_3$	$1/\beta_1+1/\beta_2=\alpha_2$ $1+\alpha_3/(\gamma+1/\beta_1)$ $=\alpha_3\beta_3$	$\alpha_1+\alpha_2=1/\beta_2$ $1+\alpha_3/(\gamma-\alpha_1)$ $=\alpha_3\beta_3$	$1+\alpha_1/(\alpha_2-1/\beta_2)$ $=\alpha_1\beta_1$ $\gamma+1/\beta_1=\alpha_1$
Type IV-9	Type IV-10	Type IV-11	
$1+\alpha_1/(\alpha_2-1/\beta_2)$ $=\alpha_1\beta_1$ $\gamma+\alpha_2=1/\beta_2$	$1+\alpha_2/(\alpha_1-1/\beta_1)=\alpha_2\beta_2$ α_1+1/β_3 $=\gamma+1/\beta_1$	$1+\alpha_1/(\alpha_2-1/\beta_2)$ $=\alpha_1\beta_1$ $\gamma+\alpha_2=1/\beta_2+1/\beta_3$	–

TABLE II
ELECTRICAL SPECIFICATIONS OF THE WPT SYSTEM

Symbols	Value			
	Type I-2	Type II-5	Type III-2	Type IV-10
α_1, α_2, α_3	1, –, –	4.33, 4.33, –	1, 0.2, –	4.33, 4.33, –
β_1, β_2, β_3	–,1, 0.34	0.3, 0.19, 0.34	–, 6, 0.33	0.3, 1.23, 0.34
γ	3.96	3.96	3.96	3.96
L_E and C_E	30 μH and 84.4 nF			
M and L_s	0−28 μH and 127.4 μH			
f_r and C_s	100 kHz and 19.9 nF			
V_{in} and R_o	100V and 10−100 Ω			

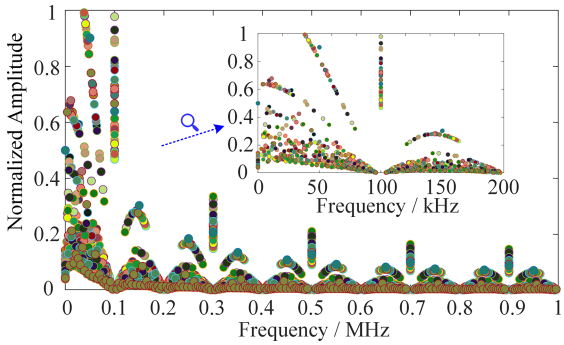

Fig. 10. Normalized amplitude of harmonic components with different voltage ratio δ, i.e., N_1 and N_3.

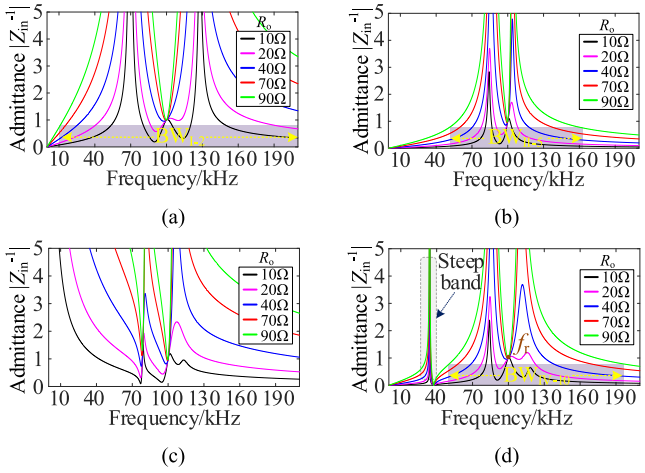

Fig. 11. Normalized input admittance of WPT systems with different PHCTs. (a) Type I-2. (b) Type II-5. (c) Type III-2. (d) Type IV-10.

combinations of N_1 and N_3, where N_1, $N_3 \subset \{23, 57, 11, 13\}$. It can be found that the amplitudes of high-order harmonics are quite small no matter what δ is. However, apart from the fundamental component at f_r (100 kHz), low-order harmonics possess relatively large amplitudes. Thus, this frequency band, in particular below 70 kHz, should be paid more attention when evaluating the band-pass characteristics of PHCT.

The normalized input admittance of WPT systems with type I-2, type II-5, type III-2, and type IV-10 PHCTs are shown in Fig. 11. By definition, the frequency range, i.e., the bandwidth BW, corresponds to a frequency value where $|Z_{\text{in}}^{-1}|$ drops by 3 dB. It can be observed from Fig. 11(a) that $\text{BW}_{\text{I-2}}$ is quite large and $|Z_{\text{in}}^{-1}|$ at low frequency is several times higher than that at f_r, especially when R_o is large. Regarding to type II-5 PHCT, as shown in Fig. 11(b), the bandwidth $\text{BW}_{\text{II-5}}$ is narrowed down and $|Z_{\text{in}}^{-1}|$ attenuates rapidly in low frequency band. This means type II-5 PHCT exhibits a good band-pass characteristic. As for type III-2 PHCT in Fig. 11(c), the $|Z_{\text{in}}^{-1}|$ curve is divergent with the decrease of frequency and it doesn't exhibit a band-pass characteristic. Regarding to type IV-10 PHCT, $\text{BW}_{\text{IV-10}}$ is comparatively narrow, as shown in Fig. 11(d). However, another steep band with high amplitude occurs around 35 kHz, as shown in the circled region. That is to say, if a large harmonic component of excitation voltage just locates near this frequency point, the inverter current may suffer from distortion, which in turn ruins ZVS operation.

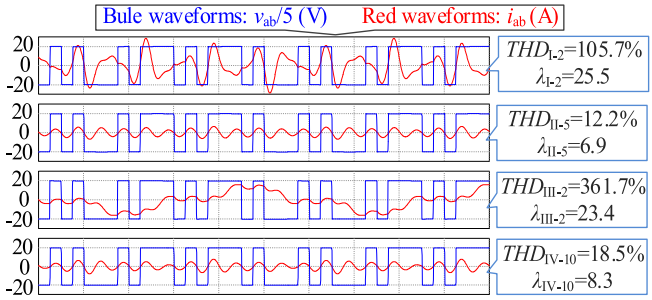

Fig. 12. Simulation results of WPT system with different PHCTs, where $\delta = 7/11$, i.e., $N_1 = 5$ and $N_3 = 2$.

Usually, the total harmonic distortion (THD) is defined as a distortion of the harmonics compared to the harmonic that is of interest (useful harmonic) [29], [30]. Here, the THD value is used to evaluate the distortion of inverter current. Moreover, a fluctuation factor λ is introduced to evaluate the oscillation of inverter current. The THD and λ values are expressed as

$$\text{THD} = \frac{I_{ab,h}}{I_{ab,fr}}, \lambda = \frac{I_{ab,pp}}{I_{\text{in}}} \tag{9}$$

where $I_{ab,h}$ is the sum of root-mean-square (rms) values of the inverter harmonic currents, $I_{ab,fr}$ is the rms value with only f_r component; $I_{ab,pp}$ is the peak-to-peak value of inverter current, and I_{in} is the input dc current. Larger THD and λ mean larger distortion and oscillation of inverter current and vice versa.

To further verify the theoretical analysis, simulation results of the WPT system with different PHCTs are given, as shown in Fig. 12, where $N_1 = 5$ and $N_3 = 2$. It can be observed that, with the same output power, inverter currents of type I-2 and type III-2 PHCTs suffer from severe distortion and ZVS is lost, where $\text{THD}_{\text{I-2}} = 105.7\%$, $\lambda_{\text{I-2}} = 25.5$, $\text{THD}_{\text{III-2}} = 361.7\%$ and $\lambda_{\text{III-2}} = 23.4$. On the contrary, the inverter currents of type II-5 and type IV-10 PHCT are almost sinusoidal and ZVS is always achieved, where $\text{THD}_{\text{II-5}} = 12.2\%$, $\lambda_{\text{II-5}} = 6.9$, $\text{THD}_{\text{IV-10}} = 18.5\%$ and $\lambda_{\text{IV-10}} = 8.3$. Obviously, the index of THD and λ of type II-5 and type IV-10 PHCTs are much smaller than that of Type I-2 and Type III-2 PHCTs.

To investigate the influence of steep band in Fig. 11(d), an excitation voltage with a large harmonic component in the steep band ($N_1 = 3$ and $N_3 = 1$) is applied to type II-5 and type IV-10 PHCTs, respectively, as shown in Fig. 13. Regarding to type IV-10 PHCT in Fig. 13(a), it can be seen that ZVS is lost and the inverter current suffers from severe distortion, where $\text{THD}_{\text{IV-10}} = 219.1\%$, $\lambda_{\text{II-5}} = 18.8$. On the contrary, for type II-5 PHCT in Fig. 13(b), ZVS operation is ensured and inverter current is almost sinusoidal with unity input power factor, where $\text{THD}_{\text{II-5}} = 16.7\%$, $\lambda_{\text{II-5}} = 6.0$. That is because the harmonic components of inverter current locating in the steep band is comparatively high in terms of type IV-10 PHCT, as indicated by the fast Fourier transform results.

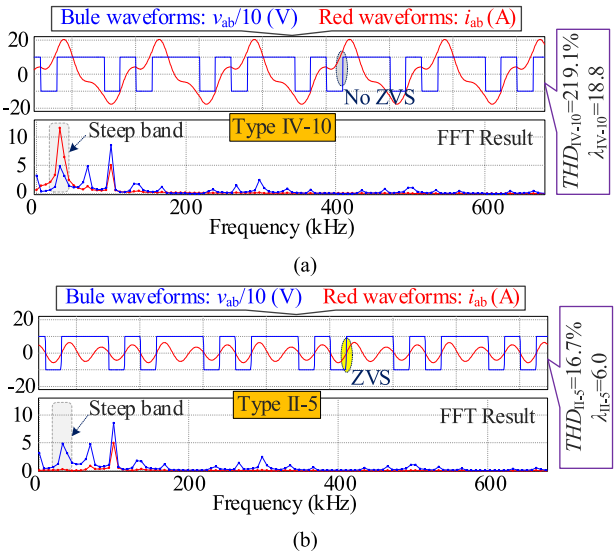

Fig. 13. Simulation results of WPT system with $\delta = 2/3$, i.e., $N_1 = 3$ and $N_3 = 1$. (a) Type IV-10 PHCT. (b) Type II-5 PHCT.

TABLE III
COMPATIBILITY BETWEEN PHCT AND SHC

Limitations	PHCTs	Performance
Without limitation on pulse distribution	II-1, II-2, II-5, IV-5	Best
Limitation on some specific pulse distribution	IV-1, IV-2, IV-4, IV-6, IV-10, IV-11	Moderate
Not applicable under any pulse distribution	I-1, I-2, I-3, II-3, II-4, II-6, II-7, II-8, III-1, III-2, III-3, III-4, III-5, III-6, III-7, IV-3, IV-7, IV-8, IV-9	Worst

In terms of the performance of WPT system when applying SHC, the aforementioned 29 PHCTs can be classified into three groups, as given in Table III. The first group PHCTs exhibit outstanding applicability to SHC in spite of the pulse distributions. That is to say, if the WPT system adopts one of these PHCTs and SHC simultaneously, the advantages of full-load range ZVS, unity input power factor, inherent open-circuit protection and high design freedom can be achieved. In terms of the second group PHCTs, a steep band exists below the resonant frequency, which may incur the potential risk of current distortion. If one of these PHCTs and SHC are jointly applied in the WPT system, ZVS operation and unity power factor may be lost under some specific pulse distribution because of the adverse effect of steep band. However, if the harmonic components of excitation voltage keep away from the steep band, the WPT system still exhibits high overall performance, possessing all the advantages mentioned in the first group PHCTs. Regarding to the third group PHCTs, if one of these PHCTs and SHC are jointly applied in the WPT system, severe current distortion cannot be avoided no matter what the pulse distribution. That is because the WPT system applying one of these PHCTs did not have a narrow band-pass characteristic, resulting in large amounts of harmonic currents in the resonant networks.

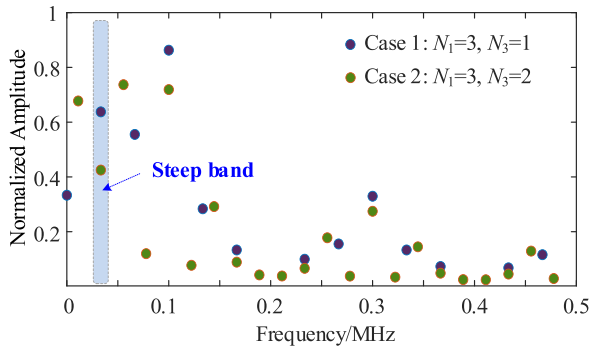

Fig. 14. DFT results of the excitation voltage with different N_1 and N_3.

C. Discussions

In this article, we firstly explore the interrelation of PHCT and SHC when they are jointly applied in a WPT system. Moreover, there are still some issues that worthy of further study.

1) Regarding to SHC in existing works, it is only applied in primary side for power regulation. Actually, it can be also used in secondary side to serve the active rectifier. For this scenario, the phase synchronization of dual-side drive signals should be paid much attention.
2) In terms of the secondary group PHCTs in Table III, there is not only a unique combination of N_1 and N_3, which may result in a poor performance of WPT system. For example, in Fig. 13, type IV-10 PHCT suffers from severe current distortion under the case $N_1 = 3$ and $N_3 = 1$. Actually, the case when $N_1 = 3$ and $N_3 = 2$ also results in a poor performance of type IV-10 PHCT. That is mainly because both cases exhibit a relatively large harmonic component of excitation voltage in the steep band, as shown in Fig. 14. The rest of possible combinations can be obtained by using the mathematical software (for instance, MATLAB).

IV. EXPERIMENTAL VERIFICATIONS

To further test the overall performance of different PHCTs in WPT system when applying SHC, an experiment prototype with 100 V input and 250 W output, as shown in Fig. 15, is built. The electrical parameters of the WPT system are given in Table IV. The outer diameter of transmitter and receiver coils are both 400 mm and the air gap is 100 mm.

Fig. 16 shows steady-state waveforms of the prototype with $N_1 = 5$ and $N_3 = 2$ when applying type I-2, type II-5, type III-2, and type IV-10 PHCTs, respectively. In Fig. 16(a), the load resistance is 10 Ω with full load output power. As can be seen, inverter currents with type I-2 and type III-2 PHCTs suffer from severe distortion and ZVS cannot be achieved. The corresponding THD and λ indexes are measured as $\text{THD}_{\text{I-2}} = 117.3\%$, $\lambda_{\text{I-2}} = 22.4$ and $\text{THD}_{\text{III-2}} = 377.1\%$, $\lambda_{\text{III-2}} = 26.4$, which are in accordance with simulation results. For type II-5

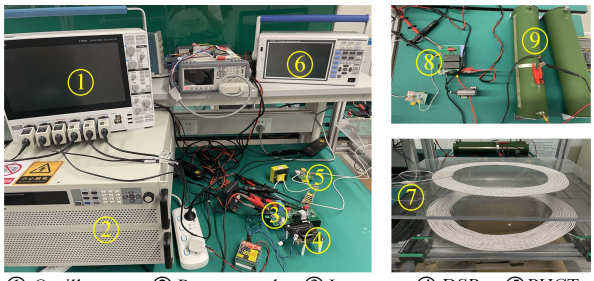

Fig. 15. Photo of experiment prototype.

TABLE IV
EXPERIMENTAL PARAMETERS OF THE WPT SYSTEM

Symbols	Value			
	Type I-2	Type II-5	Type III-2	Type IV-10
Inductance, L_1	30.3 μH	129.7 μH	30.3 μH	129.7 μH
Inductance, L_2	–	129.7 μH	6.2 μH	139.7 μH
Inductance, L_3	–	–	–	–
Capacitance, C_1	–	25.1 nF	–	25.1 nF
Capacitance, C_2	84.5 nF	15.8 nF	507.2 nF	102.4 nF
Capacitance, C_3	28.6 nF	28.6 nF	27.8 nF	28.6 nF
Self-inductance, L_p	118.5 μH	118.5 μH	118.5 μH	118.5 μH
L_E and C_E	30 μH and 84.4 nF			
M and L_s	0−28 μH and 128.6 μH			
f_r and C_s	100 kHz and 19.8 nF			

and type IV-10 PHCTs, ZVS is achieved and inverter current is almost sinusoidal with unity input power factor, where $\mathrm{THD_{II\text{-}5}} = 10.8\%$, $\lambda_{\mathrm{II\text{-}5}} = 5.7$ and $\mathrm{THD_{IV\text{-}10}} = 20.7\%$, $\lambda_{\mathrm{IV\text{-}10}} = 7.2$.

In Fig. 16(b), load resistance is 50 Ω with 20% load power. Compared with the heavy load condition in Fig. 8(a), it can be seen that the distortion of inverter currents for all four PHCTs becomes larger. However, ZVS operation are still maintained in type II-5 and type IV-10 PHCTs while lost in type I-2 and type III-2 PHCTs. The corresponding THD and λ indexes are measured as $\mathrm{THD_{I\text{-}2}} = 123.5\%$, $\lambda_{\mathrm{I\text{-}2}} = 19.8$; $\mathrm{THD_{III\text{-}2}} = 416.7\%$, $\lambda_{\mathrm{III\text{-}2}} = 20.1$; $\mathrm{THD_{II\text{-}5}} = 13.6\%$, $\lambda_{\mathrm{II\text{-}5}} = 5.5$ and $\mathrm{THD_{IV\text{-}10}} = 19.7\%$, $\lambda_{\mathrm{IV\text{-}10}} = 8.5$. To summarize, the THD and λ indexes under light load conditions is larger than that under heavy load conditions, which are consistent with the theoretical analysis in Fig. 11.

Fig. 17 shows the steady-state waveforms of the prototype applying different PHCTs under full load condition. The pulse numbers are $N_1 = 3$ and $N_3 = 1$. For the system applying type II-5 PHCT in Fig. 17(a), ZVS is achieved with unity input power factor. However, when type IV-10 PHCT is applied with the same pulse numbers, ZVS is lost and inverter current suffers from severe distortion. The THD and λ indexes are measured as $\mathrm{THD_{II\text{-}5}} = 8.6\%$, $\lambda_{\mathrm{I\text{-}2}} = 6.2$ and $\mathrm{THD_{IV\text{-}10}} = 223.7\%$, $\lambda_{\mathrm{III\text{-}2}} = 23.8$. Comparing Figs. 16 and 17, it can be deduced that the performance of Type IV-10 PHCT highly depends on the pulse distribution of SHC. That is to say, if the harmonic components of v_{ab} (determined by the pulse distribution) keep away from the steep band, the WPT system applying type IV-10 PHCT still exhibits high overall performance. Otherwise, primary inverter current suffers from severe distortion and ZVS operation is ruined as well.

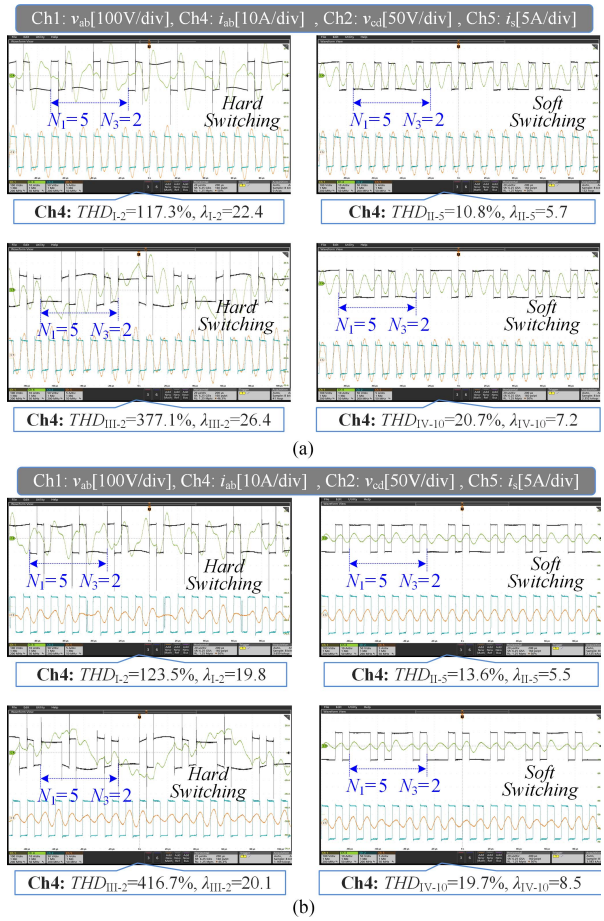

Fig. 16. Steady-state waveforms of the prototype with $N_1 = 5$ and $N_3 = 2$ when applying different PHCTs. (a) Full load condition. (b) 20% load condition.

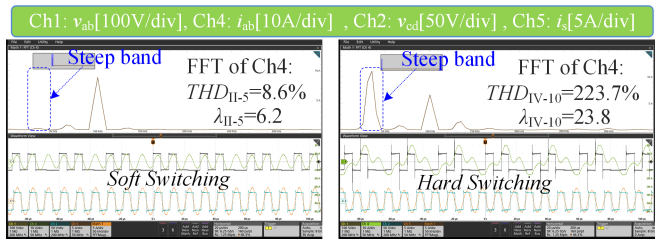

Fig. 17. Steady-state waveforms of the prototype with $N_1 = 3$ and $N_3 = 1$ when applying different PHCTs under full load condition. (a) Type II-5 PHCT. (b) Type IV-10 PHCT.

To verify the inherent open-circuit protection characteristic of PHCT, as an example, the dynamic waveforms of the WPT system applying type II-5 PHCT are shown in Fig. 18 when the receiver moves out of the operating region (M is close to zero). Apparently, inverter current decrease gradually because of the increased input impedance when the distance between the coils increases. It is evident that the proposed system can work safely when the accidental open-circuit or the absence of receiver occur.

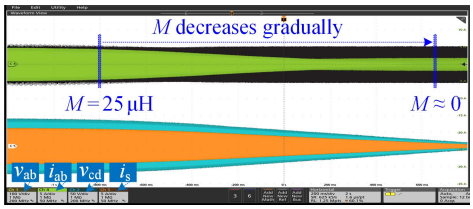

Fig. 18. Dynamic waveforms of WPT system applying type II-5 PHCT.

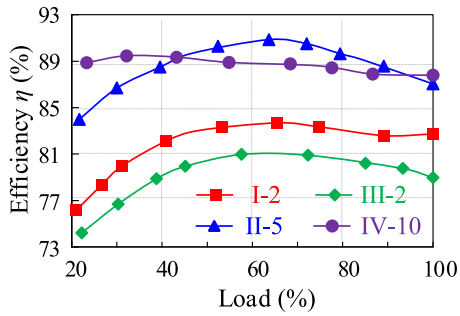

Fig. 19. Measured efficiency of SHC controlled WPT system with applying different PHCTs.

Fig. 19 shows the measured efficiency of SHC controlled WPT system applying different PHCTs, where $M = 25\ \mu$H and $\delta = 7/11$. It can be seen that the efficiencies of type II-5 and type IV-10 PHCTs are similar, and much higher than that of type I-2 and Type III-2 PHCTs. That mainly benefits from the ZVS operation and unity power factor. In addition, the overall efficiency can be improved by optimizing the circuit parameters of PHCT. For example, in terms of type II-5 PHCT, a larger L_1 leads to a smaller BW, which helps to suppress the current distortion and reduce the conduction losses. However, larger inductance means a larger equivalent series resistance of inductor, which in turn increase the conduction losses. In other words, there is a tradeoff when selecting the inductance of L_1. Similarly, the others passive components (including L_2, C_1, C_2, and C_3) in type II-5 PHCT also have influences on the overall efficiency. Therefore, the parameter optimization in terms of different PHCTs is a promising work, which will be analyzed in future works.

V. Conclusion

In this article, a systematic synthesis of PHCT is studied in terms of general T-branch structure to overcome the drawbacks of PSCT, such as low degrees of design freedom, high sensitivity to misalignments and no open-circuit protection. Based on these newly derived PHCTs, their applicability to SHC is explored by gaining insight into the filter characteristics. It is found that four kinds of PHCTs are superior over other candidates in performance because unity power factor and soft switching can be achieved without the limitation on pulse distribution. However, six kinds of PHCTs may nullify the strengths of SHC due to the adverse effects of steep band. That is to say, if the harmonic components of v_{ab} locate near the steep band, severe current distortion occurs without ZVS and unity power factor. Otherwise, they can still exhibit superior performance like the first four kind of PHCTs. The rest of PHCTs are not applicable to SHC no matter what the pulse distribution is.

References

[1] A. Ahmad, M. S. Alam, and R. Chabaan, "A comprehensive review of wireless charging technologies for electric vehicles," *IEEE Trans. Transp. Electrific.*, vol. 4, no. 1, pp. 38–63, Mar. 2018.

[2] Q. Chen, S. C. Wong, C. K. Tse, and X. Ruan, "Analysis, design, and control of a transcutaneous power regulator for artificial hearts," *IEEE Trans. Biomed. Circuits Syst.*, vol. 3, no. 1, pp. 23–31, Feb. 2009.

[3] J. H. Kim et al., "Development of 1-MW inductive power transfer system for a high-speed train," *IEEE Trans. Ind. Electron.*, vol. 62, no. 10, pp. 6242–6250, Oct. 2015.

[4] X. Wang, L. He, J. Xu, and C. K. Lee, "Widening the operating range of a wireless charging system using tapped transmitter winding and bifrequency pulse train control," *IEEE Trans. Power Electron.*, vol. 37, no. 11, pp. 13874–13883, Nov. 2022.

[5] S. Y. R. Hui and W. W. C. Ho, "A new generation of universal contactless battery charging platform for portable consumer electronic equipment," *IEEE Trans. Power Electron.*, vol. 20, no. 3, pp. 620–627, May 2005.

[6] Z. Huang, G. Wang, J. Yu, and X. Qu, "A novel clamp coil assisted IPT battery charger with inherent CC-to-CV transition capability," *IEEE Trans. Power Electron.*, vol. 36, no. 8, pp. 8607–8611, Aug. 2021.

[7] B. X. Nguyen et al., "An efficiency optimization scheme for bidirectional inductive power transfer systems," *IEEE Trans. Power Electron.*, vol. 30, no. 11, pp. 6310–6319, Nov. 2015.

[8] S. Jia, C. Chen, S. Duan, and Z. Chao, "Dual-side asymmetrical voltage-cancelation control for bidirectional inductive power transfer systems," *IEEE Trans. Ind. Electron.*, vol. 68, no. 9, pp. 8061–8071, Sep. 2021.

[9] L. Xu, Q. Chen, X. Ren, S. Wong, and C. K. Tse, "Self-oscillating resonant converter with contactless power transfer and integrated current sensing transformer," *IEEE Trans. Power Electron.*, vol. 32, no. 6, pp. 4839–4851, Jun. 2017.

[10] H. Hu, T. Cai, S. Duan, X. Zhang, J. Niu, and H. Feng, "An optimal variable frequency phase shift control strategy for ZVS operation within wide power range in IPT systems," *IEEE Trans. Power Electron.*, vol. 35, no. 5, pp. 5517–5530, May 2020.

[11] Y. Jiang, L. Wang, Y. Wang, J. Liu, M. Wu, and G. Ning, "Analysis, design, and implementation of WPT system for EV's battery charging based on optimal operation frequency range," *IEEE Trans. Power Electron.*, vol. 34, no. 7, pp. 6890–6905, Jul. 2019.

[12] U. Anwar, Z. Liu, and D. Markovic, "A burst-mode controlled inductive wireless power transfer system," in *Proc. IEEE 21st Workshop Control Model. Power Electron.*, 2020, pp. 1–6.

[13] H. Li, J. Fang, S. Chen, K. Wang, and Y. Tang, "Pulse density modulation for maximum efficiency point tracking of wireless power transfer systems," *IEEE Trans. Power Electron.*, vol. 33, no. 6, pp. 5492–5501, Jun. 2018.

[14] X. Sheng, L. Shi, and M. Fan, "An improved pulse density modulation of high-frequency inverter in ICPT system," *IEEE Trans. Ind. Electron.*, vol. 68, no. 9, pp. 8017–8027, Sep. 2021.

[15] V. Yenil and S. Cetin, "An improved pulse density modulation control for secondary side controlled wireless power transfer system using LCC-S compensation," *IEEE Trans. Ind. Electron.*, vol. 69, no. 12, pp. 12762–12772, Dec. 2022, doi: 10.1109/TIE.2021. 3134059.

[16] W. Zhong, H. Li, S. Y. R. Hui, and M. D. Xu, "Current overshoot suppression of wireless power transfer systems with on–off keying modulation," *IEEE Trans. Power Electron.*, vol. 36, no. 3, pp. 2676–2684, Mar. 2021.

[17] W. Zhong and S. Y. R. Hui, "Maximum energy efficiency operation of series-series resonant wireless power transfer systems using on-off keying modulation," *IEEE Trans. Power Electron.*, vol. 33, no. 4, pp. 3595–3603, Apr. 2018.

[18] W. Liu, K. T. Chau, C. H. T. Lee, W. Han, X. Tian, and W. H. Lam, "Full-range soft-switching pulse frequency modulated wireless power transfer," *IEEE Trans. Power Electron.*, vol. 35, no. 6, pp. 6533–6547, Jun. 2020.

[19] J. Tang, Q. Zhang, C. Cui, T. Na, and T. Hu, "An improved hybrid frequency pacing modulation for wireless power transfer systems," *IEEE Trans. Power Electron.*, vol. 36, no. 11, pp. 12365–12374, Nov. 2021.

[20] Z. Hua, K. T. Chau, W. Han, W. Liu, and T. W. Ching, "Output-controllable efficiency-optimized wireless power transfer using hybrid modulation," *IEEE Trans. Ind. Electron.*, vol. 69, no. 5, pp. 4627–4636, May 2022.

[21] X. Wang, J. Xu, M. Leng, H. Ma, and S. He, "A hybrid control strategy of LCC-S compensated WPT system for wide output voltage and ZVS range with minimized reactive current," *IEEE Trans. Ind. Electron.*, vol. 68, no. 9, pp. 7908–7920, Sep. 2021.

[22] J. L. Villa, J. Sallan, J. F. S. Osorio, and A. Llombart, "High- misalignment tolerant compensation topology for ICPT systems," *IEEE Trans. Ind. Electron.*, vol. 59, no. 2, pp. 945–951, Feb. 2012.
[23] J. Lu, G. Zhu, D. Lin, S.-C. Wong, and J. Jiang, "Load-independent voltage and current transfer characteristics of high-order resonant network in IPT system," *IEEE J. Emerg. Sel. Topics Power Electron.*, vol. 7, no. 1, pp. 422–436, Mar. 2019.
[24] R. He, P. Zhao, M. Fu, Y. Liu, H. Wang, and J. Liang, "Decomposition and synthesis of high-order compensated inductive power transfer systems for improved output controllability," *IEEE Trans. Microw. Theory Techn.*, vol. 67, no. 11, pp. 4514–4523, Nov. 2019.
[25] C. Li, W. Xu, and T. Tayjasanant, "Interharmonics: Basic concepts and techniques for their detection and measurement," *Elect. Power Syst. Res.*, vol. 66, no. 1, pp. 39–48, 2003.
[26] Y. Wang, Y. Yao, X. Liu, D. Xu, and L. Cai, "An LC/S compensation topology and coil design technique for wireless power transfer," *IEEE Trans. Power Electron.*, vol. 33, no. 3, pp. 2007–2025, Mar. 2018.
[27] Z. Dongye et al., "An S-CLC compensated load-independent inductive power relay system with constant voltage outputs," *IEEE Trans. Power Electron.*, vol. 36, no. 5, pp. 5157–5168, May 2021.
[28] A. Testa et al., "Interharmonics: Theory and modeling," *IEEE Trans. Power Del.,* vol. 22, no. 4, pp. 2335–2348, Oct. 2007.
[29] D. Shmilovitz, "On the definition of total harmonic distortion and its effect on measurement interpretation," *IEEE Trans. Power Del.*, vol. 20, no. 1, pp. 526–528, Jan. 2005.
[30] O. Dordevic, M. Jones, and E. Levi, "Analytical formulas for phase voltage RMS squared and THD in PWM multiphase systems," *IEEE Trans. Power Electron.*, vol. 30, no. 3, pp. 1645–1656, Mar. 2015.

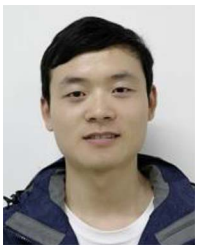

Xiaoqiang Wang received the B.Eng. and Ph.D. degrees in electrical engineering from Southwest Jiaotong University, Chengdu, China, in 2016 and 2021, respectively.

From May 2021 to February 2022, he was a Research Assistant with the Department of Electrical and Electronic Engineering, The University of Hong Kong, Hong Kong. He is currently a Postdoctoral Research Fellow with Zhejiang University, Hangzhou, China. His research interests include wireless power transfer, high-efficiency/high-power-density converters, soft switching technology, and wide bandgap devices.

Minrui Leng received the B.S. degree in electronic and information engineering and the Ph.D. degree in electrical engineering from Southwest Jiaotong University, Chengdu, China, in 2014 and 2021, respectively.

She is currently an Assistant Professor with the School of Electrical Engineering, Sichuan University, Chengdu, China. Her research interests include small signal modeling and dynamical modeling of power converter, control techniques of power converter, stability of distributed power systems and model predictive control, and cyberattacks of dc microgids.

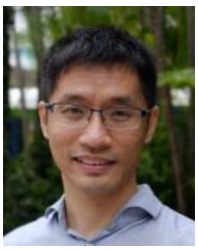

Xin Zhang (Senior Member, IEEE) received the Ph.D. degree in automatic control and systems engineering from the University of Sheffield, Sheffield, U.K., in 2016 and the Ph.D. degree in electronic and electrical engineering from Nanjing University of Aeronautics and Astronautics, Nanjing, China, in 2014.

From February 2014 to December 2016, he was a Research Associate with the University of Sheffield. From January 2017 to September 2017, he was the Postdoctoral Research Fellow with the City University of Hong Kong. From September 2017 to August 2020, he was an Assistant Professor of power engineering with the School of Electrical and Electronic Engineering, Nanyang Technological University, Singapore. He is currently a Professor with Zhejiang University, Hangzhou, China. He is generally interested in power electronics, power system, and advanced control theory, together with their applications in various sectors.

Hao Ma (Senior Member, IEEE) received the B.S, M.S, and Ph.D. degrees from Zhejiang University, Hangzhou, China, in 1991, 1994, and 1997, respectively, all in electrical engineering.

Since 1997, he has been a Lecturer, an Associate Professor, and Professor with Zhejiang University, Hangzhou, China. From September 2007 to September 2008, he was a Delta Visiting Scholar with the North Carolina State University. He is the Vice Dean of the ZJU-UIUC Institute, Urbana, IL, USA. His current research interests include advanced control in power electronics, wireless power transfer, fault diagnosis of power electronic circuits and systems, and application of power electronics.

Bin Guo was born in Hubei, China, in 1992. He received the B.S. degree in electrical engineering from Beihua University, China, in 2015 and the Ph.D. degree in control science and engineering from Central South University, Changsha, China, in 2021.

He is currently a Postdoctoral Research Fellow with Zhejiang University, Hangzhou, China. His research interests include modeling and control of power electronics, PV renewable energy and energy storage system, multilevel inverters.

Jianping Xu (Member, IEEE) received the B.S. and Ph.D. degrees in electronic engineering from the University of Electronics Science and Technology of China, Chengdu, China, in 1984 and 1989, respectively.

Since 1989, he has been with the School of Electrical Engineering, Southwest Jiaotong University, Chengdu, China, where he has been a Professor since 1995. From November 1991 to February 1993, he was with the Department of Electrical Engineering, University of Federal Defense Munich, Germany, as a Visiting Research Fellow. From February 1993 to July 1994, he was with the Department of Electrical Engineering and Computer Science, University of Illinois at Chicago, Chicago, IL, USA, as a Visiting Scholar. His research interests include the modeling, analysis, and control of power electronic systems.

Chi-Kwan Lee (Senior Member, IEEE) received the B.Eng. and Ph.D. degrees in electronic engineering from the City University of Hong Kong, Hong Kong, in 1999 and 2004, respectively.

He is currently an Associate Professor with the Department of Electrical and Electronic Engineering, The University of Hong Kong, Hong Kong. He was a Lecturer of electrical engineering with The Hong Kong Polytechnic University, Hong Kong. From 2010 to 2020, he was a Visiting Researcher with Imperial College London, England, U.K. His current research interests include inductive power transfer, metamaterials for wireless power, and application of machine learning in design of electromagnetic devices.

Dr. Lee was a recipient of the 2015 IEEE Power Electronics Society Transactions First Prize Paper Award for his publications on Wireless Power Transfer. He serves on the steering committee and was the General Chair of 2018 IEEE PELS Workshop on Emerging Technologies: Wireless Power. He is an Associate Editor for IEEE TRANSACTIONS ON POWER ELECTRONICS and IEEE JOURNAL OF EMERGING AND SELECTED TOPICS IN POWER ELECTRONICS.